Electronic Supplementary Material (ESI) for Green Chemistry.

Supplementary Information

Metal-exchanged magnetic β zeolites: valorization of lignocellulosic biomass-derived compounds to platform chemicals

Erlen Y. C. Jorge,[a,b] Thiago de M. Lima,[a] Carolina G. S. Lima,[a] Lucas Marchini,[a] William N. Castelblanco,[c] Daniel G. Rivera,[b] Ernesto A. Urquieta-González,[a,c] Rajender S. Varma*[d] and Márcio W. Paixão*[a]

[a]*Centre of Excellence for Research in Sustainable Chemistry (CERSusChem), Department of Chemistry, Federal University of São Carlos – UFSCar, Rodovia Washington Luís, km 235 - SP-310, São Carlos, São Paulo, Brazil-13565-905.*
E-mail: mwpaixao@ufscar.br

[b]*University of Havana, Institute of Science and Technology of Materials, Zapata and G, Centro Habana, Havana 10400, Cuba*

[c]*Department of Chemical Engineering, Federal University of São Carlos - UFSCar, Rodovia Washington Luís, km 235 - SP-310, São Carlos, São Paulo, Brazil-13565-905.*

[d]*Regional Centre of Advanced Technologies and Materials, Departments of Physical Chemistry and Experimental Physics, Faculty of Science, Palacky University, 783 71 Olomouc, Czech Republic*

General Methods. All solvents were dried prior to use by standard procedures. Reagents were purchased at the highest commercial quality and used without further purification. The particle size and morphological studies of the Fe_3O_4 microspheres used as support and the catalysts were performed by Transmission Electron Microscopy (TEM), which was carried out using a FEI TECNAI G^2 F20 microscope. For the TEM analyses, the powder samples were dispersed in ethanol and -sonicated for 5 min. One drop of this solution was placed on a 400 mesh copper grid with carbon film and the sample was dried at room temperature. The XRD measurements were performed in a Rigaku Miniflex Diffractometer using the K_α radiation of a Cu source (λ=1,54187 Å), 40 kV, 30 mA and 2θ in the range of 5° to 80° and a rate of 2° min^{-1}.

The Rietveld refinement[1] was performed in order to quantify the different crystalline phases present in the beta zeolite samples. For that, the diffractogram of the sodic form of magnetic beta zeolite was obtained using a Rigaku Geiger-Flex diffractometer with a graphite monochromator in the 2θ range of 5° to 100° using a CuKα source and a step scan of 0.02° and 6 s by step. The Rietveld refinement was carried out using the space groups $P4_122$ for beta zeolite [JCPDS 48-0074], C12/m1 for ZSM-12 zeolite [JCPDS 86-2364], and $P2_13$ for maghemite [JCPDS 04-0755] and using the software GSAS,[2] which uses the least-squares method to reach the best agreement between the experimental and the calculated diffraction profiles. The quality of the Rietveld refinement was accessed through the R values and χ^2. X-Ray fluorescence (XRF) analyses were performed in a PANalytical MiniPal 4 spectrometer equipped with a Rh X-ray tube operating at 4 kW.

Samples were analyzed using a Shimadzu GCMS-QP2010S Gas Chromatograph coupled to a MS detector equipped with an Zebron ZB5-MS capillary column (30 m x 0.32 mm, 0.25 µm) under the operation parameters: temperature of inlet of 250 °C, temperature of the interface of 300 °C, temperature ramp of the oven from 50 to 250 °C at a rate of 10 °C min^{-1}.

The XPS analyses were conducted in a UNI-SPECS UHV spectrometer with a base pressure below $5x10^{-7}$ Pa. The Al Kα line was used ($h\nu$ = 1486.6 eV) as ionization source, and the analyzer pass energy was set to 10 eV. The inelastic noise of the high-resolution spectra Fe2p, Ir4f and Pd3d, was subtracted using the Shirley method. The composition was determined from the relative areas corrected using the Scofield atomic sensitivity factor with a ±5% precision. The spectra were deconvoluted using a Voight-type function, combined with Gaussian and Lorentz. The FWHM varied between 1,4 and 2,1 eV, and the position of the peaks was determined with a ±0,1 eV precision.[3]

TPD measurements were conducted in a Micromeritics Autochem II 2920 Chemisorption Analyzer equipment with a TCD (Thermal Conductivity Detector) detector. For this, 50 mg of the sample were pre-treated thermally under 30 mL min^{-1} helium flow at a heating rate of 10 °C min^{-1} until 600 °C and kept at this temperature for 30 minutes. After this period, the reactor was cooled to 120 °C, and the He flow was kept for 60 minutes. Next, the adsorption of ammonia was performed through the passing of a 15% mixture of NH_3 in He for 30 minutes over the sample. After saturation, the sample was purged with He for 1 hour to remove the excess of ammonia. Finally, the temperature desorption was initiated under a 30 mL min^{-1} He flow in a 15 °C min^{-1} heating rate until 600 °C. To quantify the acid sites, the area under the curve of the graph of TCD signal x temperature was calculated.

The infrared spectrum of absorbed pyridine was recorded on a Fourier Transform Infrared spectrophotometer model Prestigi-21 in the range of 1800–1400 cm^{-1}. For the qualitative acidity determination, 50 mg of sample were subjected to a heat treatment in a tubular furnace at 300 °C and 100 mL min^{-1} N_2 flow for 1 h. Gaseous pyridine was then adsorbed on the samples for 1 h at 150 °C with a N_2 gas carrier flow at 100 mL min^{-1}. Next, the N_2 flow was kept constant for 1 h at 150 °C for the removal of the physically adsorbed pyridine.

ICP-OES measurements were conducted in a Thermo Fisher Scientific, iCAP 6300 Duo, with a CID (Charge Injection Device) detector.

The nitrogen sorption measurements were performed using a Micromeritics equipment model ASAP 2020. Before the measurements, the powdered samples were previously treated at 200 °C for 2 h under vacuum aiming to remove adsorbed water. After that, the powders were analyzed with gaseous nitrogen adsorption at -196 °C and the volume of micropores and the external area were determined using the t-plot method.[4]

The Mossbauer characterization were carried out using a standard spectrometer at room temperature and a ^{57}Co as radioactive source dissolved in Rh matrix. The measurements were carried out using a transmission geometry without external magnetic field.

The magnetic measurements were carried out using and apparatus combining a superconducting quantum interference device and a vibrating sample magnetometer model Quantum Design MPMS SQUID-VSM. The magnetization was measured as function of the applied magnetic field (MxH) at room temperature and up to 70 kOe.

Characterization of the support and the magnetically recoverable transition metal-exchanged catalysts

Figure S1 shows the TEM image in which a statistical particle count was performed (the figure is identical to the one depicted as Figure 2a in the manuscript) - the particle size distribution was plotted as a histogram, which is showed in Figure S2.

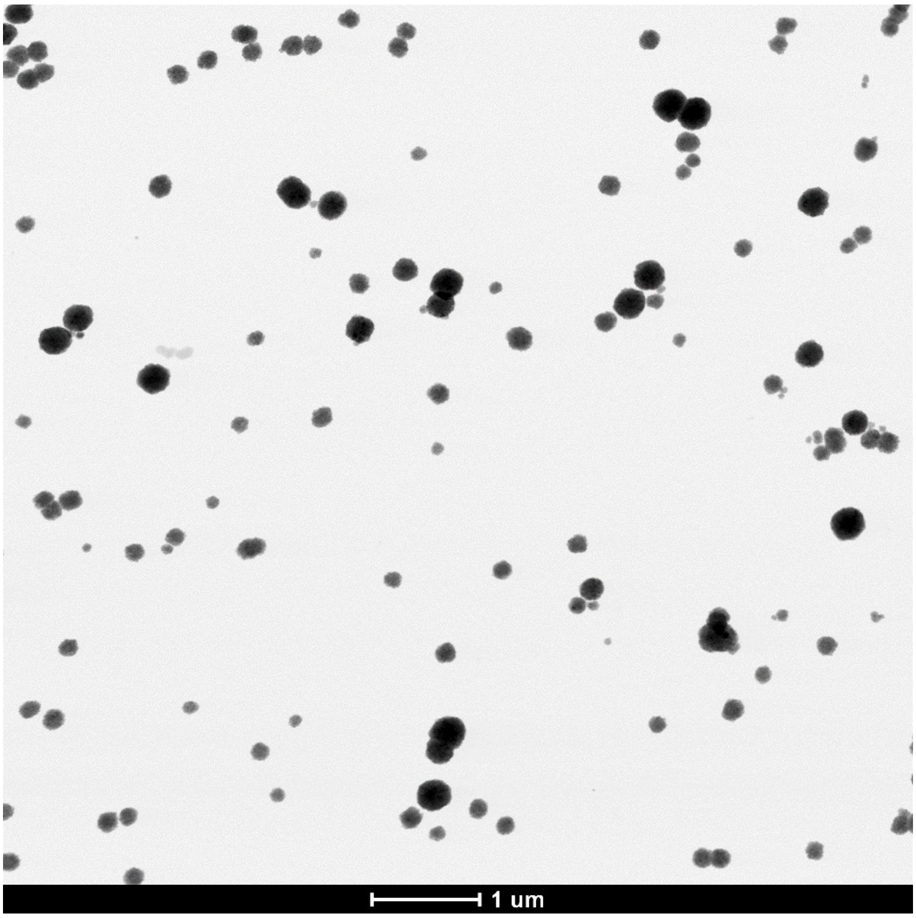

Figure S1. TEM image used for the determination of the particle size distribution (also depicted in the manuscript as Figure 2a).

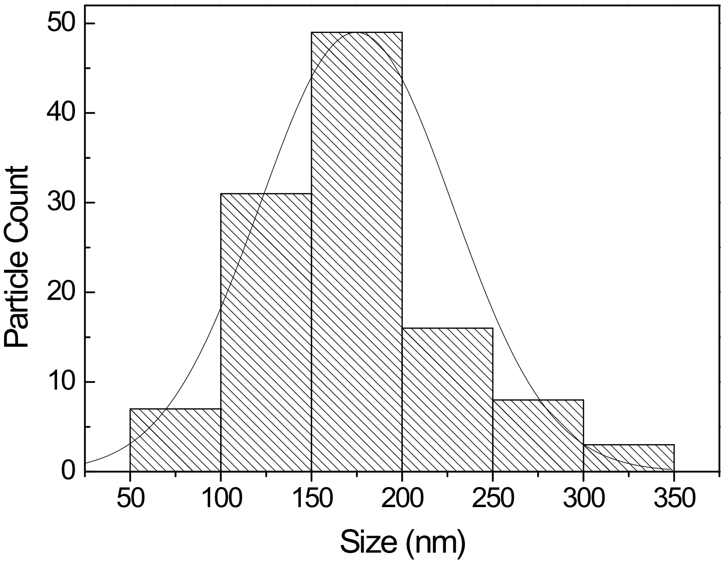

Figure S2. Histogram showing the particle size distribution constructed from the TEM image depicted in Figure S1.

The particles present in the surface of the Pd-exchanged catalyst were also counted in the image depicted in Figure S3 (the same as Figure 3b in the manuscript) and had their size distribution plotted as a histogram (Figure S4).

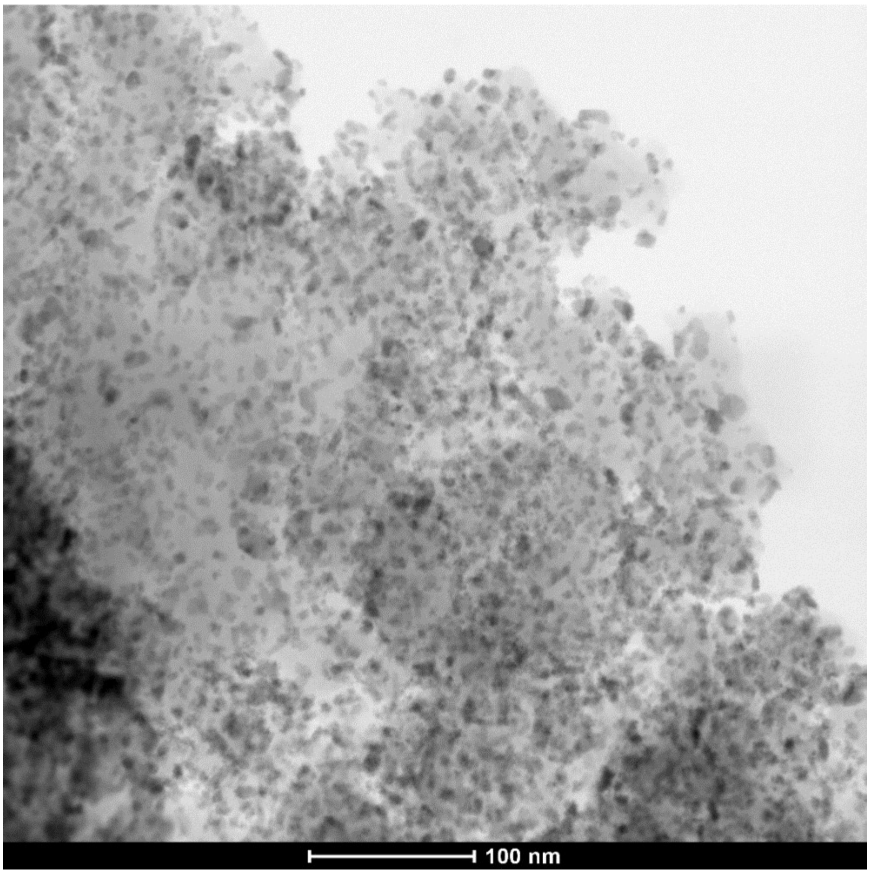

Figure S3. TEM image used for the determination of the particle size distribution of the Pd nanoparticles on the surface of the Pd-exchanged catalyst (also depicted in the manuscript as Figure 3b).

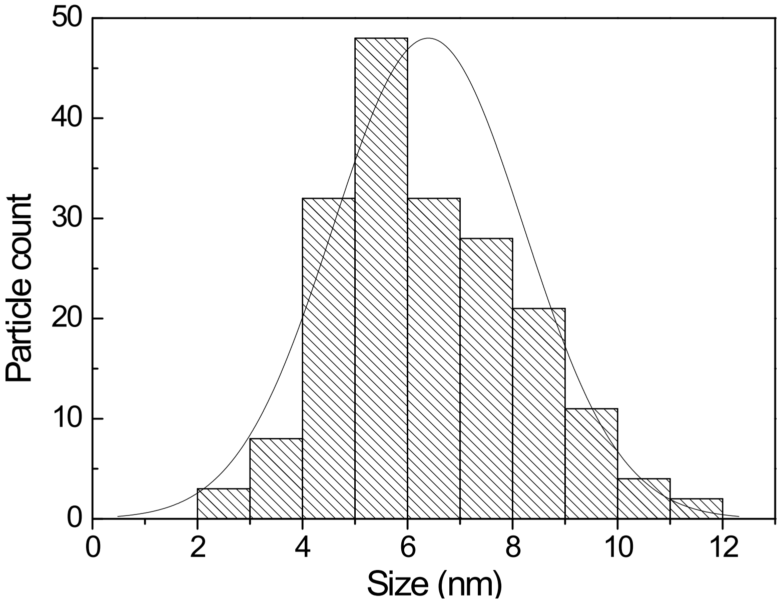

Figure S4. Histogram showing the particle size distribution constructed from the TEM image depicted in Figure S3.

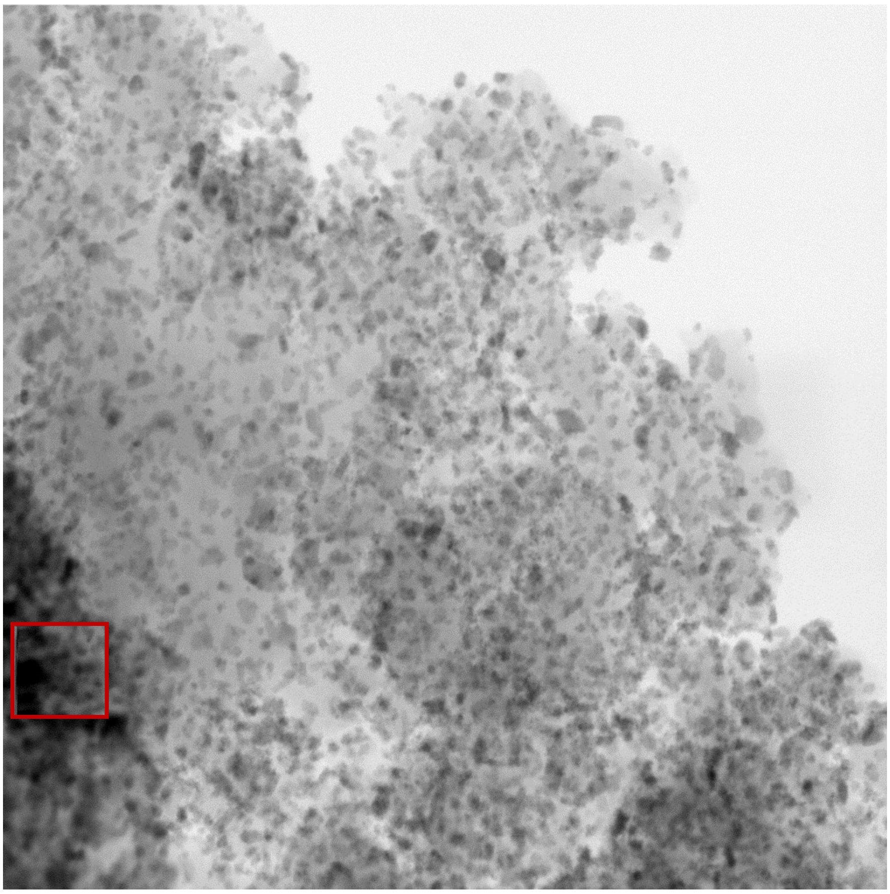

Figure S5. Image of the Pd-exchanged catalyst showing the delimited square area are in which the EDX analysis was performed.

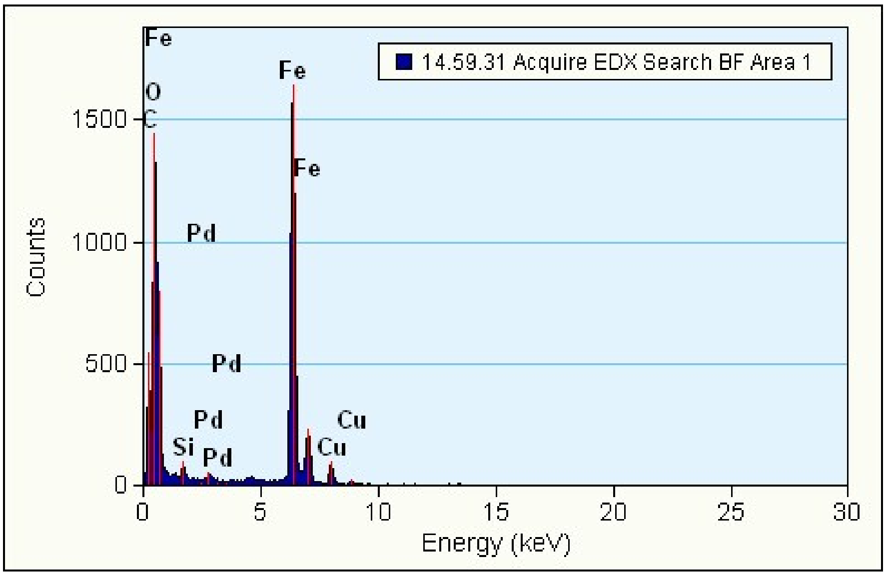

Figure S6. EDX analysis performed in the delimited square area depicted in image S5.

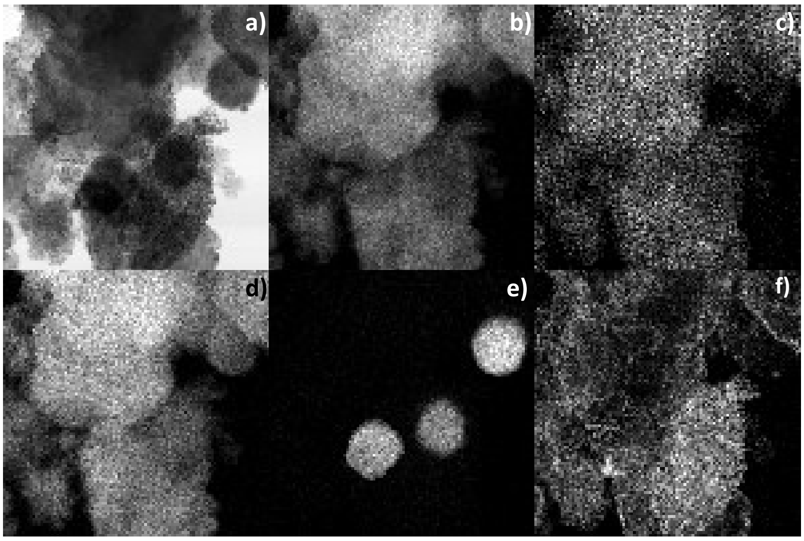

Figure S7. a) Bright-Field TEM image of the Pd-exchanged catalyst and elemental mapping of b) Si, c) Al, d) O, e) Fe and f) Pd.

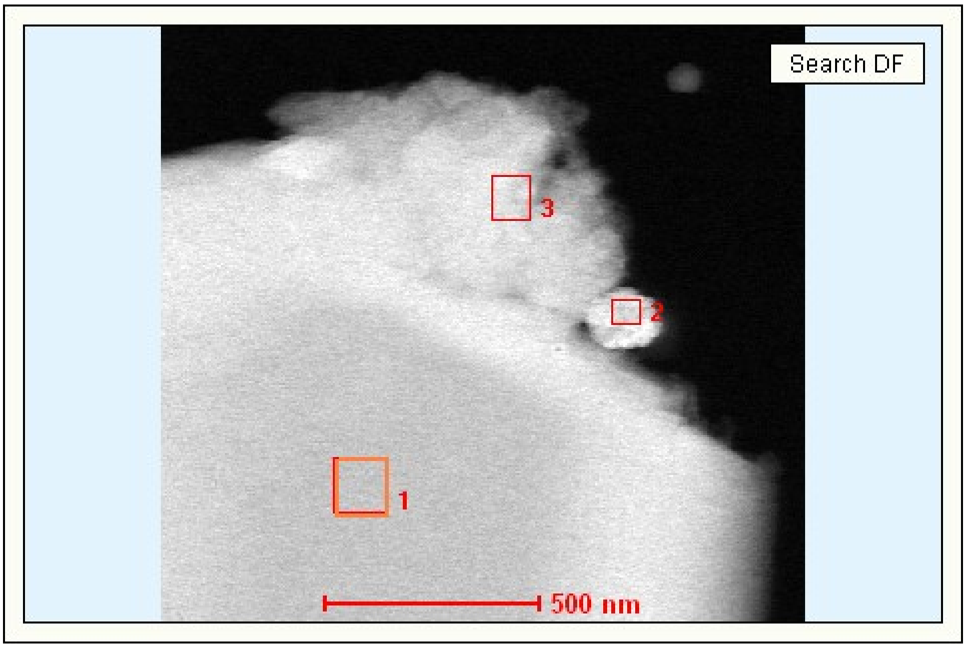

Figure S8. Image of the Fe-exchanged catalyst showing the delimited square areas in which the EDX analyses were performed.

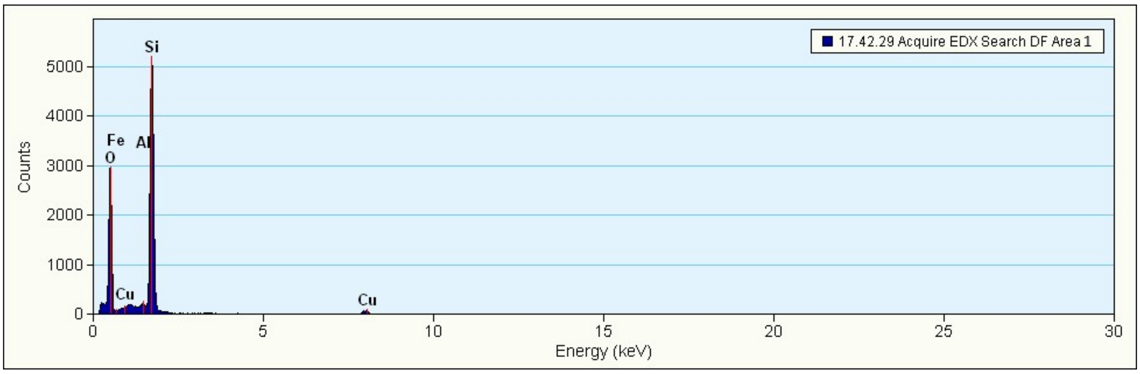

Figure S9. EDX analysis performed in the delimited square area 1 of image S8.

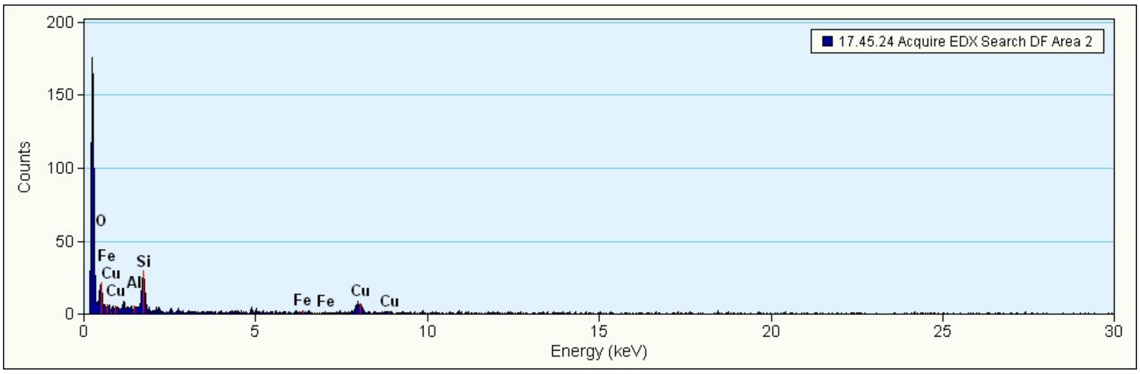

Figure S10. EDX analysis performed in the delimited square area 2 of image S8.

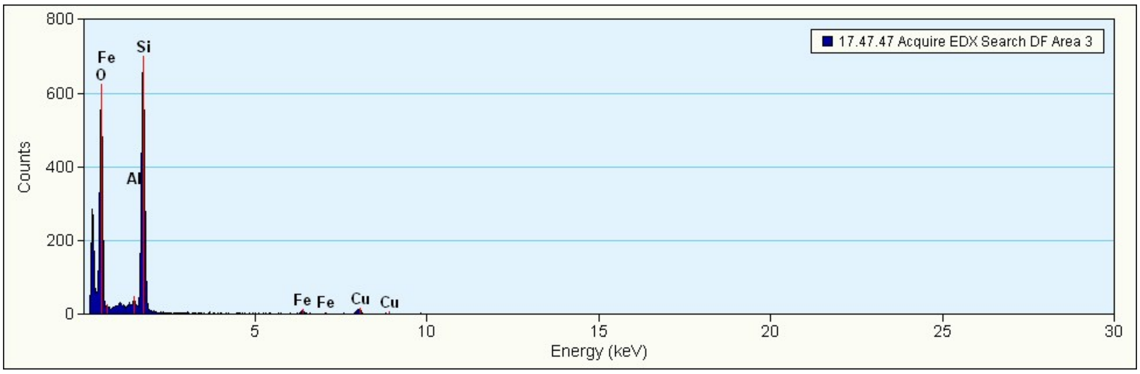

Figure S11. EDX analysis performed in the delimited square area 3 of image S8.

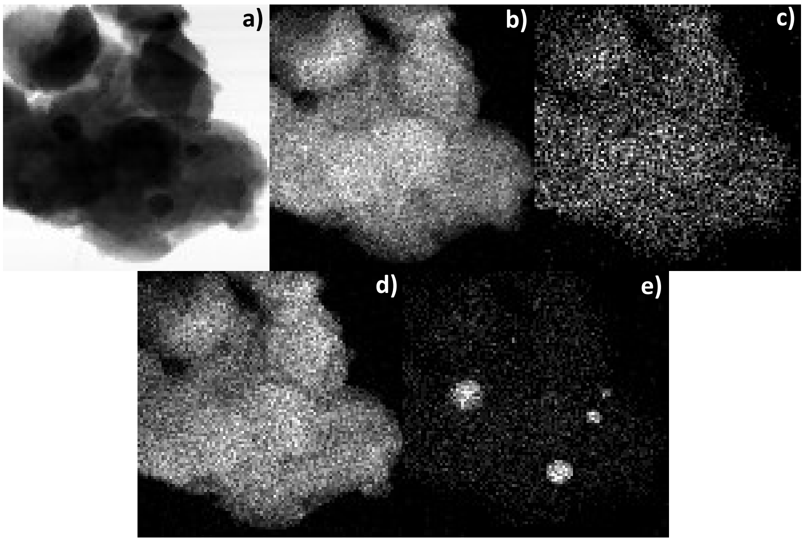

Figure S12. a) Bright-field TEM image of the Fe-exchanged catalyst and elemental mapping of b) Si, c) Al, d) O and e) Fe.

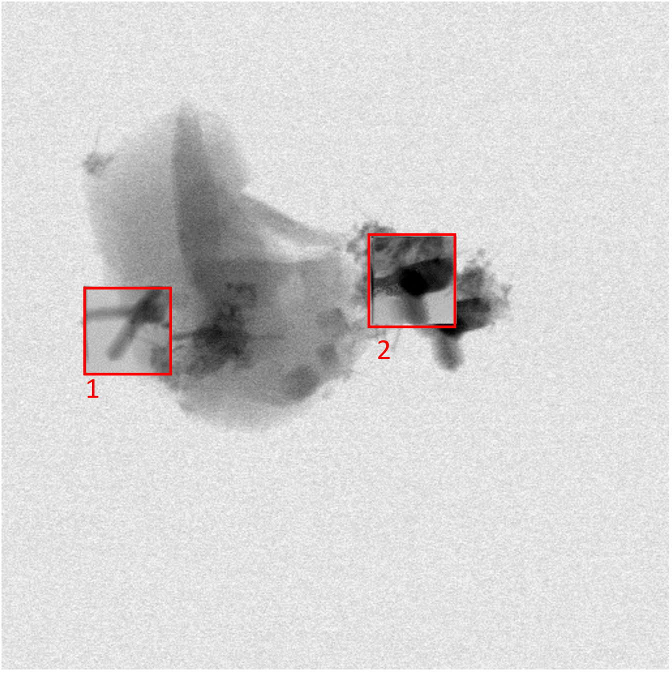

Figure S13. Image of the Ir-exchanged catalyst showing the delimited square areas in which the EDX analyses were performed.

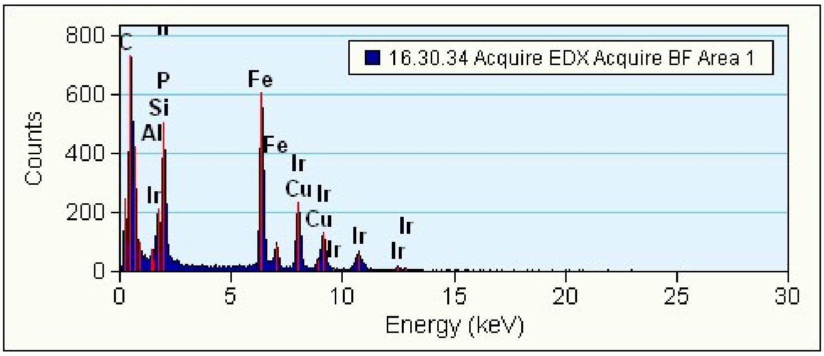

Figure S14. EDX analysis performed in the delimited square area 1 of image S13.

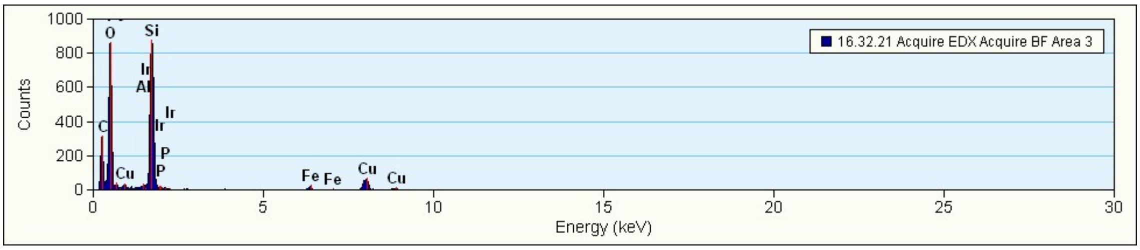

Figure S15. EDX analysis performed in the delimited square area of image S13.

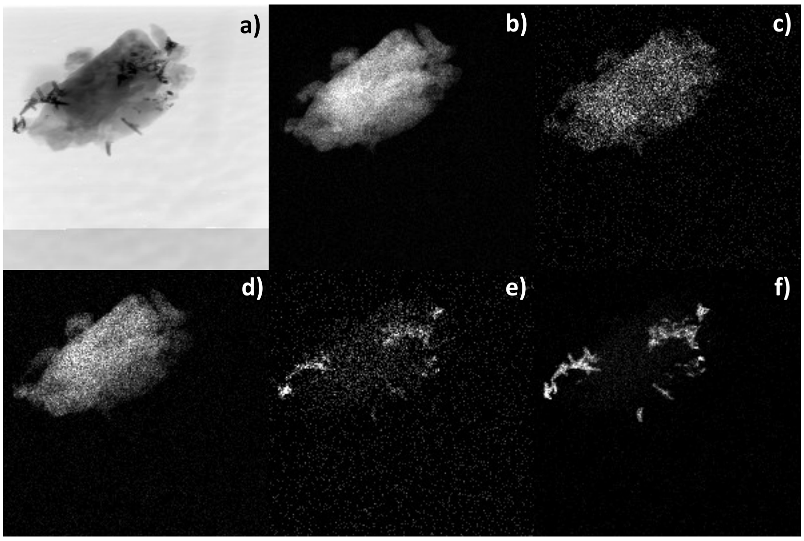

Figure S16. a) Bright-Field TEM image of the Ir-exchanged catalyst and elemental mapping of b) Si, c) Al, d) O, e) Fe an f) Ir.

Table S1. Total acidity of the metal-exchanged catalysts determined by temperature programmed desorption of ammonia NH_3-TPD.

Catalyst	**Total Acidity (μmol of NH_3/g of catalyst)**
γ-Fe_2O_3-β-H^+	1315.5
γ-Fe_2O_3-β-Pd	1807.6
γ-Fe_2O_3-β-Ir	1685.9
γ-Fe_2O_3-β-Fe	1919.5

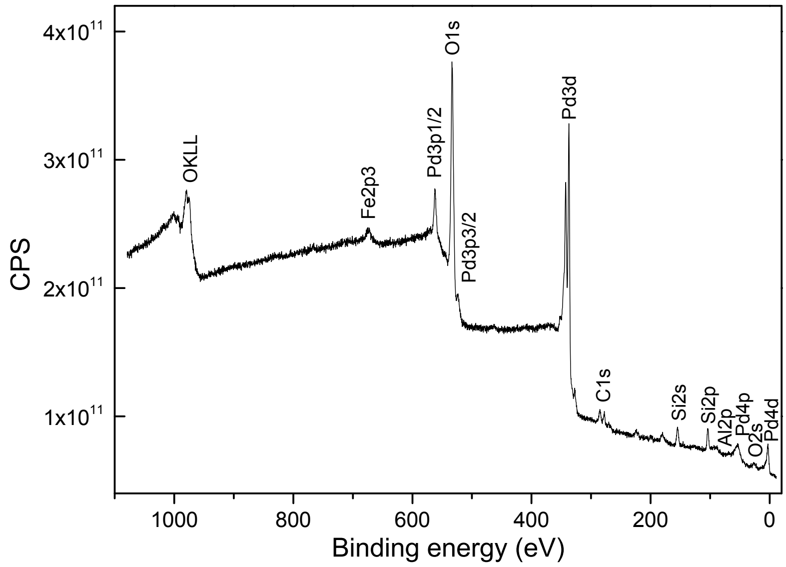

Figure S17. XPS spectrum for the Pd-exchanged catalyst.

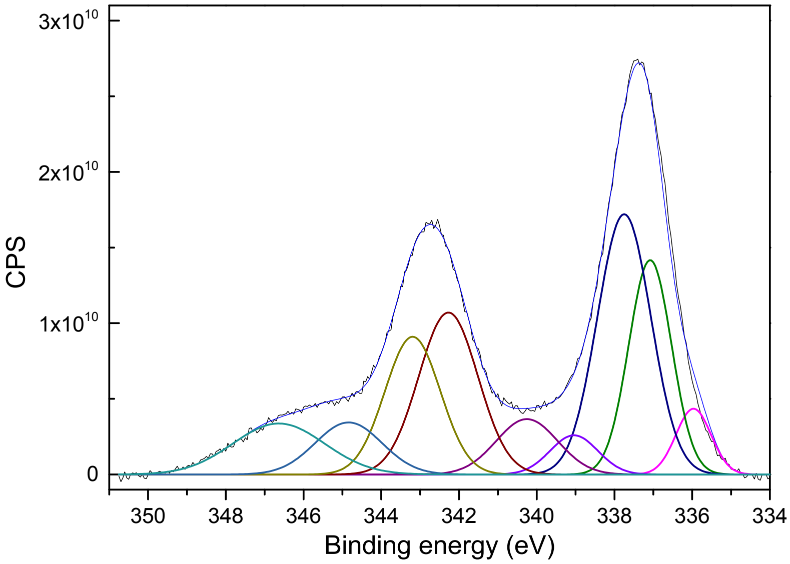

Figure S18. Pd3d core level XPS spectrum for the Pd-exchanged catalyst.

Table S2. The relative quantitative amount of each Pd species in the surface of the Pd-exchanged zeolite.

Core level	Binding Energy	Species	Area
Pd3d	335.96	Pd^{2+}	8.6%
	337.08	Pd^{+}, PdO	33.6%
	337.75	PdO_2	50.9%
	339.04	Pd^{3+}	6.9%

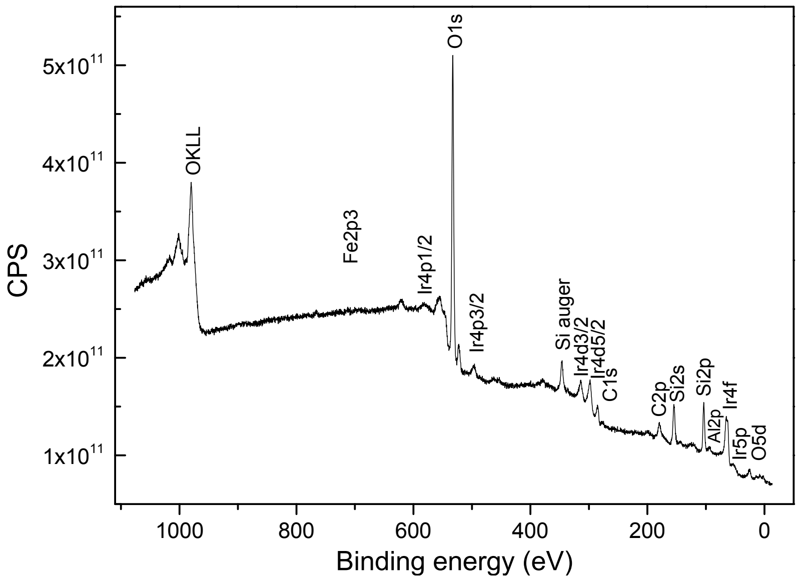

Figure S19. XPS spectrum for the Ir-exchanged catalyst.

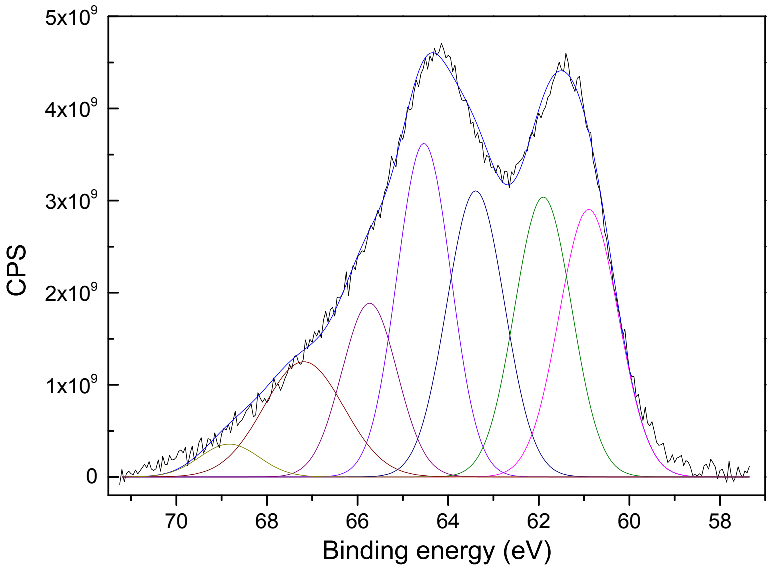

Figure S20. Ir4f core level XPS spectrum for the Ir-exchanged catalyst.

Table S3. The relative quantitative amount of each Ir species in the surface of the Ir-exchanged zeolite.

Core level	Binding Energy	Species	Area
Ir4f	61.90	Ir^{3+}	32.8%
	63.39	Ir^{4+}	35.6%
	64.53	IrO_2	31.6%

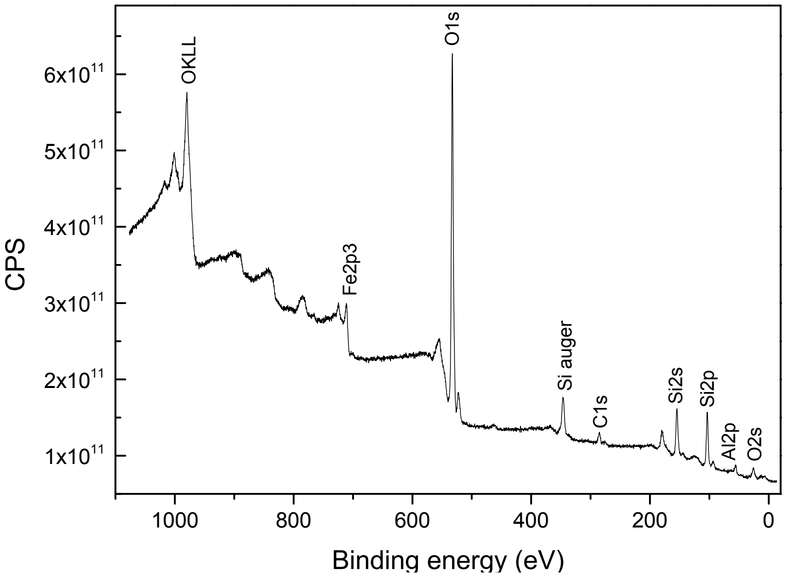

Figure S21. XPS spectrum for the Fe-exchanged catalyst.

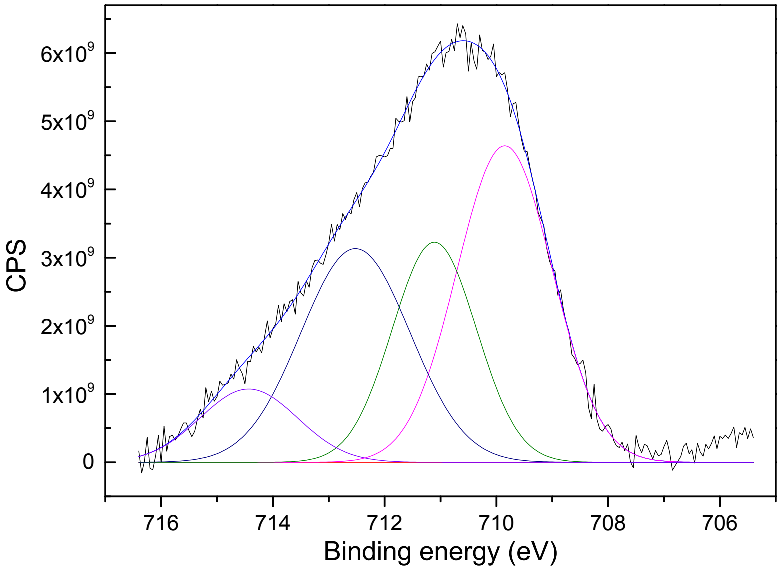

Figure S22. Fe2p core level XPS spectrum for the Fe-exchanged catalyst.

Table S4. The relative quantitative amount of each Fe species in the surface of the Fe-exchanged zeolite.

Core level	Binding Energy	Species	Area
Fe2p	709.85	Fe^{2+} (Fe_3O_4)	41.9%
	711.11	Fe^{3+} (γ-Fe_2O_3)	25.7%
	712.52	Fe^{3+}	32.4%

Figure S23 shows the Rietveld refinement of the magnetic beta zeolite in the sodium form, in which the phase 1 is assigned to the beta zeolite (BEA structure), phase 2 assigned to the ZSM-12 zeolite (MTW structure) and phase 3 is referred to maghemite (γ-Fe_2O_3). It is noteworthy to mention that the values of Rwp, Rp, $R(F^2)$ and χ^2 were 0.0781, 0.0489, 0.0615 and 1.202 respectively, being quite satisfactory to achieve a good refinement. Based on this, the obtained values for the weight fractions were 60.52%, 33.97% and 5.51% for beta zeolite, ZSM-12 zeolite and γ-Fe_2O_3, respectively.

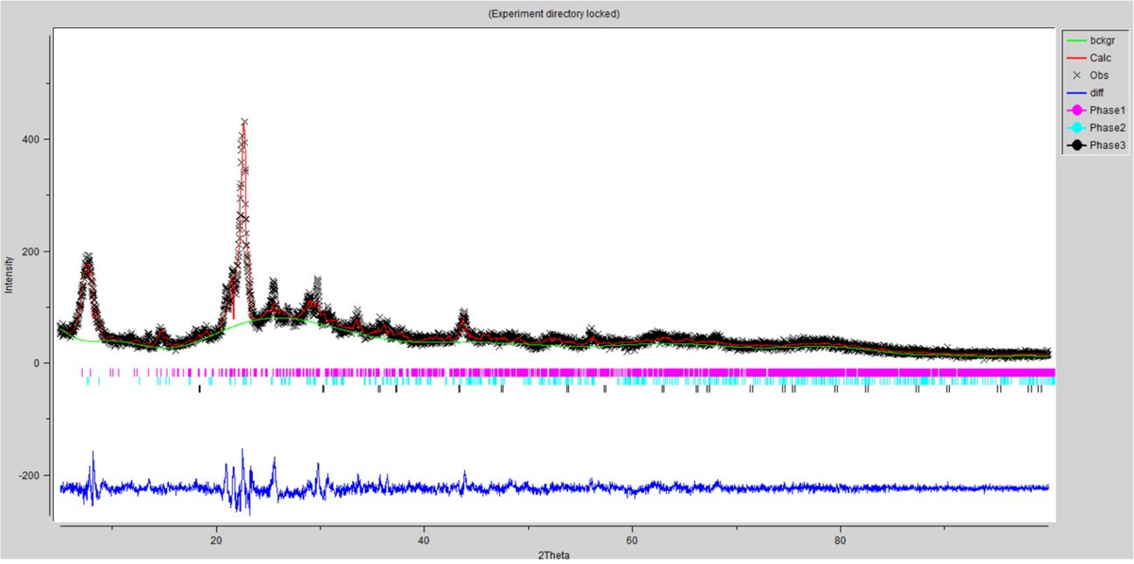

Figure S23. Rietveld refinement of the magnetic beta zeolite in the sodium form.

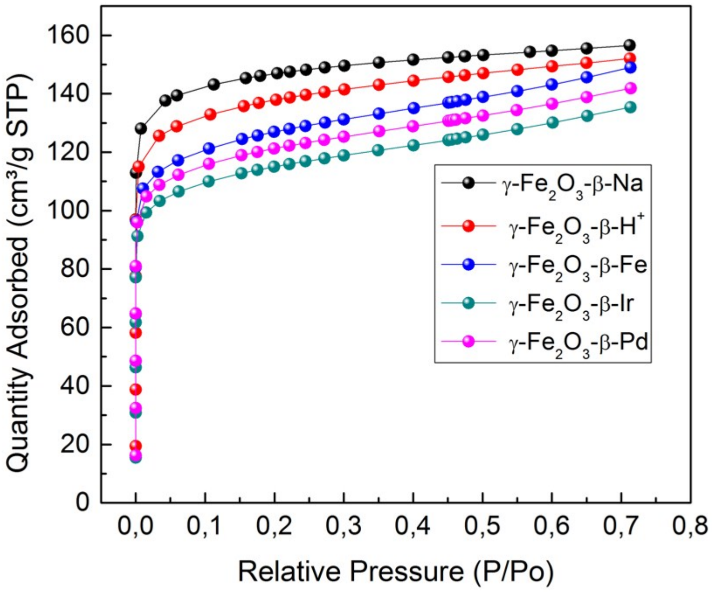

Figure S24. Nitrogen sorption curves of the zeolite in the sodium form and of the metal-exchanged catalysts.

Table S5. Specific surface area and micropore volume of the zeolite in the sodium form and of the metal-exchanged catalysts.

Sample	Specific Surface Area ($m^2\ g^{-1}$)	Micropore Volume ($cm^3\ g^{-1}$)
γ-Fe_2O_3-β-Na	398	0.190
γ-Fe_2O_3-β-H^+	358	0.138
γ-Fe_2O_3-β-Fe	296	0.142
γ-Fe_2O_3-β-Ir	283	0.136
γ-Fe_2O_3-β-Pd	285	0.137

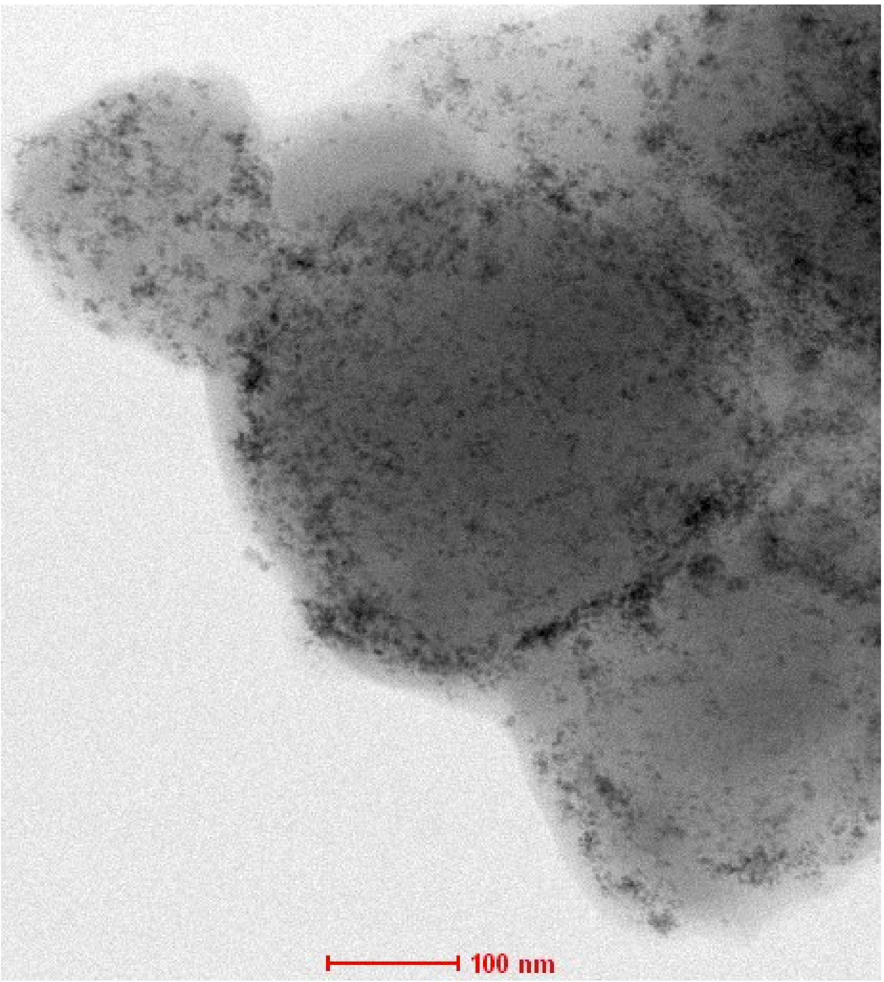

Figure S25. TEM image of the Pd-exchanged catalyst after the reaction.

Catalytic evaluation: valorization of ethyl levulinate using a combination of the catalyst in the acid form and exchanged with Fe

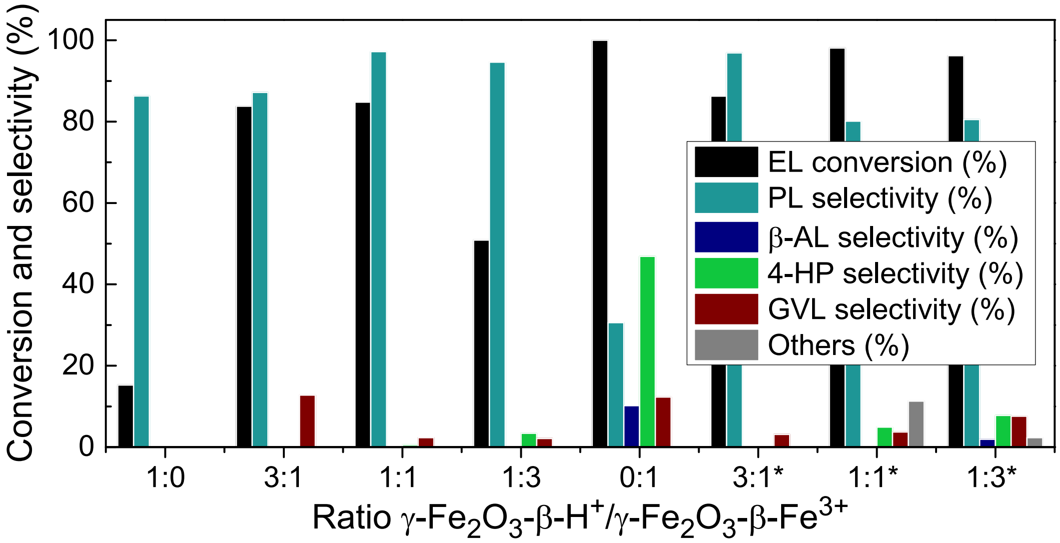

Figure S26. Upgrading of ethyl levulinate in the presence of different ratios of the catalyts γ-Fe_2O_3-β-H^+/γ-Fe_2O_3-β -Fe^{3+}. *Reactions performed at 150°C. EL = ethyl levulinate, PL = isopropyl levulinate, β-AL = β-angelica lactone, 4-HP = isopropyl 4-hydroxypentanoate, GVL = γ-valerolactone. Reaction conditions: 0.3 mmol of ethyl levulinate, 750 μL of isopropyl alcohol and different amounts of catalyst at 130°C for 24h.

Characterization and the catalytic evaluation of the catalysts with the separate pure zeolites

In order to understand how each zeolite could affect the catalytic activity of the catalyst, a set of catalysts comprised by each zeolite separately was prepared, as well as a catalyst with a physical mixture in the same proportion of that of the synthetized catalyst were prepared.

To accomplish that, the pure zeolites were initially prepared using techniques described in the literature, as follows:

Synthesis of pure beta zeolite

The synthesis of pure beta zeolite was performed using an adaptation of the procedure described by Camblor et al, using TEAOH (40 wt.% in water) as template, fumed silica (Aerosil 200) as silica source and sodium aluminate as aluminum source. Firstly, a solution containing 5.94 mL of distilled water, 8.96 g of TEAOH and 0.053 g of sodium chloride was prepared, followed by the addition of 2.95 of Aerosil 200 silica and stirring for 20 min. Next, a solution containing 10.0 mL of distilled water, 0.033 g of sodium hydroxide and 0.179 g of sodium aluminate was prepared and added to the previously prepared silica mixture. A thick gel with theoretical molar composition of $1.97\ Na_2O:1.00\ K_2O:12.5(TEA)_2O:Al_2O_3:50\ SiO_2:750\ H_2O:2.9HCl$ was obtained, stirred for 30 min and transferred to a 100 mL Teflon-lined autoclave. The gel was hydrothermally treated at 140 °C for 5 days and the resulting powder was filtrated and washed thoroughly with distilled water, dried at 80 °C for 12 h and calcined in air atmosphere at 550 °C for 6 h.

Synthesis of pure ZSM-12 zeolite

The synthesis of pure ZSM-12 zeolite was performed according the procedure described by Gopal et al, using TEAOH (40 wt.% in water) as template, coloidal silica LUDOX (40 wt.%) as silica source and sodium aluminate as aluminum source. For the preparation of the gel, 8.75 mL of TEAOH were mixed with 8.5 mL of distilled water and 0.343 g of sodium aluminate, and this mixture was stirred until the sodium aluminate was dissolved. Next, a solution containing 19.2 mL of colloidal silica and 10.0 mL of distilled water was added to the above solution and stirred for 30 min. After that, the gel with a theoretical composition of Na_2O:Al_2O_3:80SiO_2:12.7TEAOH:104H_2O was transferred to a 100 mL Teflon-lined autoclave and hydrothermally treated at 160 °C for 5.5 days. The solid was then filtrated and washed thoroughly with distilled water and dried at 80 °C for 12 h, followed by calcination in air at 600 °C for 6 h.

Initially, the pure zeolites were characterized in their sodium form by XRD in order to confirm their identity and crystallinity (Figure S27). The x-ray diffractogram of both zeolites showed their characteristic diffraction peaks.[6,7]

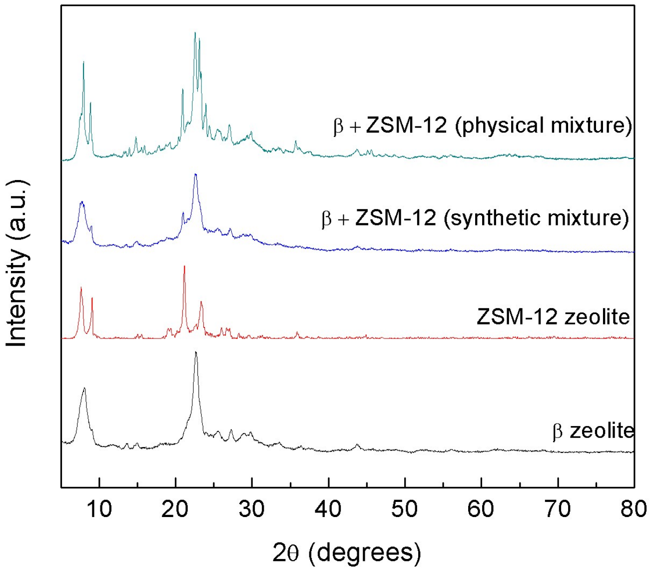

Figure S27. XRD of the pure zeolites and of the physical and synthetic mixture in the sodium form.

Later on, X-ray fluorescence analyses were conducted in order to determine the Si/Al ratio of the different zeolites. The obtained values, listed in table S6, are in accordance with the expected theoretical ones.

Table S6. Si/Al ratio for the pure zeolites and the synthetic mixture determined by X-ray fluorescence.

Sample	**Si/Al ratio**
β zeolite	23
ZSM-12 zeolite	76
β + ZSM-12 (synthetic mixture)	34

With the pure zeolites fully characterized in hand, the catalysts with the corresponding zeolites were prepared as follows:

Preparation of the catalyst with the pure β zeolite - γ-Fe_2O_3-β(p)-Pd

70 mg of the PDDA-functionalized magnetite microspheres were dispersed in 12 mL of distilled water with the subsequent addition of 500 mg of the pure β zeolite powder and stirring for 48 h at room temperature. The resulting composite Fe_3O_4-PDDA-β(p)-Na^+ was magnetically separated from the aqueous mixture and dried at 60 °C for 24 h under vacuum. The material was then calcinated under air atmosphere at 550 °C for 5 h, affording the composite γ-Fe_2O_3-β(p)-Na^+. 250 mg of the Fe_3O_4-PDDA-β(p)-Na^+ were dispersed in 5 mL of distilled water followed by the addition of $Pd(NO_3)_2.H_2O$ to attain a Pd concentration of 0,01 mol L^{-1}. The mixture was stirred at room temperature for 6h, the solid was removed via magnetic decantation and dried at 60 °C for 12 h. This ion exchange procedure was repeated twice more. Finally, the obtained powder was calcinated at 550 °C for 5h.

Preparation of the catalyst with the pure ZSM-12 zeolite - γ-Fe_2O_3-ZSM-12-Pd

70 mg of the PDDA-functionalized magnetite microspheres were dispersed in 12 mL of distilled water with the subsequent addition of 500 mg of the pure ZSM-12 zeolite powder and stirring for 48 h at room temperature. The resulting composite Fe_3O_4-PDDA-ZSM-12-Na^+ was magnetically separated from the aqueous mixture and dried at 60 °C for 24 h under vacuum. The material was then calcinated under air atmosphere at 550 °C for 5 h, affording the composite γ-Fe_2O_3-β(p)-Na^+. 250 mg of the Fe_3O_4-PDDA-ZSM-12-Na^+ were dispersed in 5 mL of distilled water followed by the addition of $Pd(NO_3)_2.H_2O$ to attain a Pd concentration of 0,01 mol L^{-1}. The mixture was stirred at room temperature for 6h, the solid was removed via magnetic decantation and dried at

60 °C for 12 h. This ion exchange procedure was repeated twice more. Finally, the obtained powder was calcinated at 550 °C for 5h.

Preparation of the catalyst with the physical mixture of β and ZSM-12 zeolites - γ-Fe_2O_3-(β+ZSM-12)-Pd

Approximately 70 mg of the PDDA-functionalized magnetite microspheres were dispersed in 12 mL of distilled water with the subsequent addition of a mixture of 320 mg of pure β zeolite and 180 mg of ZSM-12 zeolite, followed by stirring for 48 h at room temperature – this proportion was used based on the results obtained from the Rietveld refinement of the catalyst obtained as a synthetic mixture of the mentioned zeolites. The resulting composite Fe_3O_4-PDDA-(β+ZSM-12)-Na^+ was magnetically separated from the aqueous mixture and dried at 60 °C for 24 h under vacuum. The material was then calcinated under air atmosphere at 550 °C for 5 h, affording the composite γ-Fe_2O_3-PDDA-(β+ZSM-12)-Na^+. 250 mg of γ-Fe_2O_3-PDDA-(β+ZSM-12)-Na^+ were dispersed in 5 mL of distilled water followed by the addition of $Pd(NO_3)_2.H_2O$ to attain a Pd concentration of 0,01 mol L^{-1}. The mixture was stirred at room temperature for 6h, and the solid was removed via magnetic decantation and dried at 60 °C for 12 h. This ion exchange procedure was repeated twice more. Finally, the obtained powder was calcinated at 550 °C for 5h.

Characterization of the catalysts

In order to verify if the morphology of the obtained catalysts was similar to the one obtained as a synthetic mixture of zeolites, TEM analyses were carried out. The TEM images (Figure S28a and b) of the three catalysts with the pure zeolites and with the physical mixture of the zeolites (Figure 28c) in the same proportion as in the initial γ-Fe_2O_3-β-Pd catalyst have showed the all catalysts display very similar morphologies, and those are very similar to the one of the γ-Fe_2O_3-β-Pd catalyst (see image 3a in the manuscript).

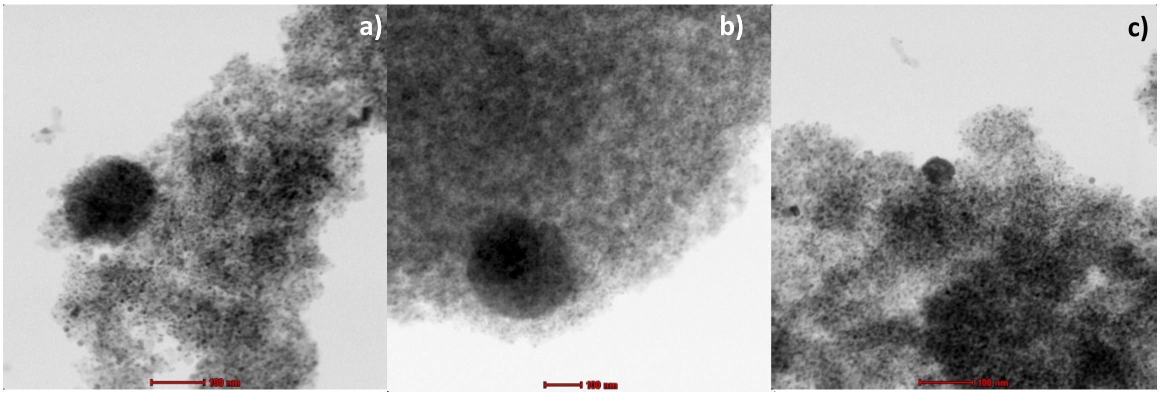

Figure S28. TEM imagem of a) γ-Fe_2O_3-β(p)-Pd, b) γ-Fe_2O_3-ZSM-12-Pd and c) γ-Fe_2O_3-(β+ZSM-12)-Pd.

Next, aiming to verify the acid properties of the different catalysts, NH_3-TPD (Table S7) and FT-IR of adsorbed pyridine analyses (Figure S29) were performed. As expected, the total acidity for the catalyst comprised by the physical mixture of zeolites is very close to the one obtained for the catalyst γ-Fe_2O_3-β-Pd, which is a synthetic mixture of the zeolites in the same proportion. The γ-Fe_2O_3-β(p)-Pd catalyst, which was prepared from the pure β zeolite, was the one with the highest acidity, and that may be rationalized considering its lower Si/Al ratio and its higher Pd content; a similar inference can be made for the γ-Fe_2O_3-ZSM-12-Pd catalyst, which has the lowest acidity and Pd content, a direct consequence of its Si/Al ratio. As for the catalysts with the mixture of zeolites, both the synthetic and physical mixtures had similar acidity and Pd content.

Table S7. Total acidity of the metal-exchanged catalysts determined by temperature programmed desorption of ammonia NH_3-TPD.

Catalyst	**Total Acidity (μmol of NH_3/g of catalyst)**	**Si/Al ratio**	**Pd% (%wt)**
γ-Fe_2O_3-β(p)-Pd	1887	23	2.6
γ-Fe_2O_3-ZSM-12-Pd	1199	76	0.8
γ-Fe_2O_3-(β+ZSM-12)-Pd	1830	40	1.2
γ-Fe_2O_3-β-Pd	1808	34	1.1

As for the FT-IR of adsorbed pyridine, all catalysts showed both Lewis and Brønsted type acid sites, but catalyst γ-Fe_2O_3-ZSM-12-Pd showed a considerably higher amount of weak Brønsted acid sites, a consequence of its high silicon content combined with the relatively lower Pd amount.

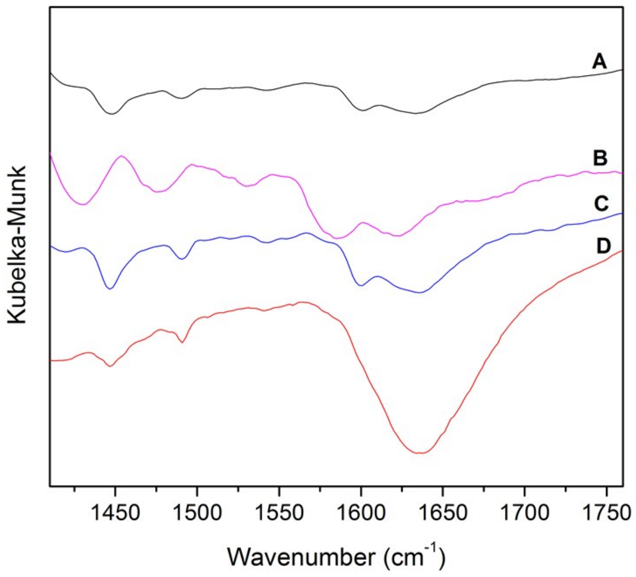

Figure S29. Fourier transform infrared spectroscopy of adsorbed pyridine spectra of the magnetically recoverable catalysts. A = γ-Fe_2O_3-(β+ZSM-12)-Pd, B = γ-Fe_2O_3-β-Pd, C = γ-Fe_2O_3-β(p)-Pd and D = γ-Fe_2O_3-ZSM-12-Pd.

Next, the catalysts were submitted to the conversion of furfural and furfuryl alcohol to isopropyl levulinate following the optimized reaction conditions, as follows:

Procedure for the catalytic evaluation – preparation of isopropyl levulinates from furfural or furfuryl alcohol using the γ-Fe_2O_3-(β+ZSM-12)-Pd, C = γ-Fe_2O_3-β(p)-Pd and γ-Fe_2O_3-ZSM-12-Pd catalysts

0.3 mmol of the starting material (furfural or furfuryl alcohol), 750 µL of isopropyl alcohol for the reaction with furfural or 230µL for the reaction with furfuryl alcohol and 75 mg of the magnetically recoverable catalyst were added to a glass vial containing a magnetic stir bar. The vial was sealed and immersed in a pre-heated oil bath at 130 °C and magnetically stirred at 700 rpm for 24h for the reaction with furfural or ethyl levulinate or for 21h for the reaction with furfuryl alcohol.

Delightfully, all catalysts afforded full conversion of both furfural and furfuryl alcohol, with complete selectivity to isopropyl levulinate. The high activity of the γ-Fe_2O_3-ZSM-12-Pd even with a lower Pd content and acidity can be rationalized considering its high micropore sizes, combined with the great amount of Brønsted acid sites in its structure. Those observations confirm our initial suspicions that the presence of ZSM-12 in the catalysts does not have a deleterious effect in their catalytic activity, quite the contrary.

References

1. H. M. Rietveld, *J. Appl. Crystallogr.* 1969, **2**, 65-71.

2. B. H. Toby, *J.Appl. Crystallogr.* 2001, **34**, 210-213.

3. (a) D. Briggs, M.P. Seah, Practical Surface Analysis, Vol. 1 Auger and X-ray Photoelectron Spectroscopy, John Wiley & Sons, Chichester, Reino Unido, 1990. (b) G.C. Smith, Surface Analysis by Electron Spectroscopy, Plenum, New York, Estados Unidos, 1994. (c) J.H. Scofield, *J. Electron Spectrosc.,* 1996, 8, 129-137. (d) J.F. Moulder, W.F. Stickle, P.E. Sobol, K.D. Bomben, Handbook of X-ray photoelectron spectroscopy, edited by J. Chastain, Perkin-Elmer Corporation, Physical Electronics Division, Eden Prairie, Minnesota, Estados Unidos, 1992. (e) NIST X-ray Photoelectron Spectroscopy Database, AV. Naumkin, A. Kraut-Vass, S.W. Gaarenstroom, C.J. Powell, NIST Standard Reference Database 20, v. 4.1: http://srdata.nist.gov/XPS/

4. B. C. Lippens and J. H. De Bôer, J. Catal., 1965, 4, 319-323.

5. M. A. Camblor, J. Pérez-Pariente, Zeolites, 1991, 11, 202-210.

6. S. Loiha, S. Prayoonpokarach, P. Songsiriritthigun, J. Wittayakun, *Mater. Chem. Phys.*, 2009, **115**, 637-640.

7. S. Gopal, K. Yoo, P. G. Smirniotis, *Micropor. Mesopor. Mater.*, 2001, **49**, 149-156.